New variants of AADC deficiency expand the knowledge of enzymatic phenotypes

[a1]Riccardo Montioli, [a1]Giovanni Bisello, [b]Mirco Dindo, [c]Giada Rossignoli, [a]Carla Borri Voltattorni and [a§]Mariarita Bertoldi

[a]Department of Neuroscience, Biomedicine and Movement Sciences, Section of Biological Chemistry, University of Verona, Strada Le Grazie, 8, 37134 Verona, Italy

[b]Okinawa Institute of Science and Technology Graduate University, 1919-1 Tancha, Onna-son Okinawa 904-0412, Japan

[c]Molecular Neurosciences, Developmental Neurosciences Programme, UCL Great Ormond Street Institute of Child Health, 30 Guildford Street, London, WC1N 1EH, UK

[§]corresponding author: mita.bertoldi@univr.it

[1]equal contribution

ABSTRACT

AADC deficiency is a rare genetic disease caused by mutations in the gene of aromatic amino acid decarboxylase, the pyridoxal 5'-phosphate dependent enzyme responsible for the synthesis of dopamine and serotonin. Here, following a biochemical approach together with an *in silico* bioinformatic analysis, we present a structural and functional characterization of 13 new variants of AADC. The amino acid substitutions are spread over the entire protein from the N-terminal (V60A), to its loop1 (H70Y and F77L), to the large domain (G96R) and its various motifs, i.e. loop2 (A110E), or a core β-barrel either on the surface (P210L, F251S and E283A) or in a more hydrophobic *milieu* (L222P, F237S and W267R) or loop3 (L353P), and to the C-terminal domain (R453C). Results show that the β-barrel variants exhibit a low solubility and those belonging to the surface tend to aggregate in their apo form, leading to the identification of a new enzymatic phenotype for AADC deficiency. Moreover, five variants of residues belonging to the large interface of AADC (V60A, G96R, A110E, L353P and R453C) are characterized by a decreased catalytic efficiency. The remaining ones (H70Y and F77L) present features typical of apo-to-holo impaired transition. Thus, defects in catalysis or in the acquirement of the correct holo structure are due not only to specific local domain effects but also to long-range effects at either the protein surface or the subunit interface. Altogether, the new characterized enzymatic phenotypes represent a further step in the elucidation of the molecular basis for the disease.

Keywords: pyridoxal 5'-phosphate enzymes, aromatic amino acid decarboxylase deficiency, AADC deficiency variants, structure and function relationship, protein chemistry, enzymology

Abbreviations: PLP, pyridoxal 5'-phosphate; AADC, aromatic amino acid decarboxylase; Dopa, 3,4-dihydroxyphenylalanine

1. Introduction

Aromatic amino acid decarboxylase (AADC) deficiency is a rare autosomic disease first reported by Hyland et al. [1, 2] nearly 30 years ago. It is caused by mutations (mainly missense but also frameshift and splicing alterations) present in homozygosis or compound heterozygosis in the gene encoding for AADC, the pyridoxal 5'-phosphate (PLP) enzyme responsible for the synthesis of dopamine and serotonin following decarboxylation of L-Dopa and 5-hydroxytryptophan [3, 4]. The disease is mainly diagnosed in infancy and exhibits many different symptoms reflecting the lack or low levels of catechol and indole biogenic amines. Patients experience several altered physiological functions such as hypotonia, hypokinesia, oculogyric crises, development and behavioural problems, autonomic dysfunctions such as nasal congestion, modified circadian rhythm, pain and temperature instability [5-10]. The present pharmacological treatment foresees a combination of pyridoxine, the precursor of PLP to keep AADC saturated with its coenzyme, monoamine oxidase inhibitors, to avoid dopamine and serotonin further depletion, and dopamine agonists, to mimic the effect of dopamine. Unfortunately, in many cases, the response is generally poor and this infantile form of Parkinsonism is particularly threatening and, in the most severe forms, leads to death in the first decade of life.

Up to now, nearly 120 patients have been identified worldwide [9], but the number is continuously growing since knowledge about this defect is increasing among child neurologists. Moreover, the extent of affected people might be even higher considering i) newly reported case of a heterozygous patient that possesses one allele with a mild mutation, while the other allele has no mutations [11], ii) another heterozygous case with typical AADC deficiency symptoms (case II-2 in [12]) and iii) a milder case of AADC deficiency reported by [13]. These unsuspected patients expand the spectrum of AADC deficiency with recent estimates [14, 15] predicting that the number of affected people is higher than reported and many patients remain not diagnosed or misdiagnosed [15].

In order to counteract AADC deficiency, some strategies have currently been undertaken. Firstly, a gene therapy approach has been carried out in Taiwan by Dr. Hwu and co-workers [16-19] and in Japan [20] with some patients, leading to some benefits but still not decisive improvements. Secondly, mouse models with different genetic defects have been generated to simulate AADC deficiency and understand the human disease [21-24], but much has still to be done.

A biochemical research of genotype to phenotype correlation has been carried out in order to elucidate the molecular basis of an altered phenotype by characterizing the related enzymatic variant. Previously, the structural/functional correlation of the effects of mutations for 16 AADC variants were studied [25]. This approach deepened the understanding of the role played by

individual amino acids on enzyme structure and function, suggesting more effective therapeutic interventions.

After five years the number of identified mutations has rapidly increased. The total number of the identified *AADC* mutations leading to the disease, including missense mutations determining homozygosis or compound heterozygosis, insertions, deletions, introns and non-coding regions modifications, has been recently updated [15]. In particular, 13 new mutations have been identified in homozygosis or hemizygosis and their protein variants are listed in **Table 1**. Notably, the variants of His-70 and Ala-110 have been re-characterized since they were incorrectly reported (see **Table 1**).

On the basis of the structure of AADC, solved both in the pig holo (~ 90% sequence identity with the human enzyme) [26] and in the human apo form [27], the new sites of mutation are spread overall the entire protein and not only in the central part of each monomer as previously claimed [25] (**Fig. 1)**.

Here, by a combination of bioinformatic and physico-chemical techniques, we present a structural and functional characterization of the new homozygous and hemizygous variants of AADC. The data obtained pertain to residues that belong to: i) loop1 (aa 66-84) of the N-terminal region (H70Y and F77L), ii) the interface between monomers (V60A, G96R, A110E, L353P and R453C) and iii) different regions of the large domain (P210L, L222P, F237S, F251S, W267R and E283A). The correlation between position and functional effect represents a powerful approach for disease phenotype prediction.

2. Materials and Methods

2.1 Materials

PLP, L-Dopa, dopa methylester (DME), hydroxylamine hydrochloride, isopropyl-β-d-thiogalactopyranoside (IPTG), trinitrobenzenesulfonic acid (TNB), phenylmethylsulfonyl fluoride (PMSF), protease inhibitor cocktail (P8849), were purchased from Sigma. Anti AADC monoclonal antibody (8E8) and mouse IgG kappa binding protein (m-IgGk BP) conjugated with HRP were purchased from Santa Cruz Biotechnology.

2.2 Site-directed mutagenesis

AADC variants were obtained by mutating the template DNA on the pDDChis vector as previously described [25]. Each mutagenesis reaction has been performed using the Quick-Change II kit (Agilent technologies) using the appropriate oligonucleotides (summarized in **Table S1)** and their complements. All mutations were confirmed by DNA sequence analysis of the whole ORF.

2.3 Expression and Purification of AADC variants

E. coli BL21 (DE3) cells were transformed by heat shock at 42°C with the desired construct and grown in 4.5 L of Luria–Bertani (LB) broth in presence of ampicillin (100 mg/ml). The cultures were grown at 37°C to an OD_{600nm} of 0.4-0.6, and expression was induced with 0.1 mM IPTG for 15 h at 30°C. Cells were harvested and resuspended in 20 mM sodium phosphate buffer pH 7.4, containing 0.5 M NaCl, 20 mM imidazole, 50 μM PLP, 0.5 mM PMSF and protease inhibitor cocktail. Lysozyme was then added to a concentration of 0.2 mg/ml and the culture was incubated for 20 min at room temperature. After a freeze-thaw, leupeptin and pepstatin (both at 1μg/ml concentration) were added and the suspension was centrifuged at 16,000 g for 30 min. The crude cellular lysate was loaded on a HisPrep FF 16/10 column (GE Healthcare) equilibrated with 20 mM sodium phosphate buffer pH 7.4, containing 0.5 M NaCl and 20 mM imidazole. AADC was eluted with a linear gradient (0-100% in 200 ml) of the same buffer containing 500 mM imidazole. After addition of 50 μM PLP, the protein solution was concentrated and imidazole and unbound coenzyme were removed by extensive washing with 100 mM potassium phosphate buffer pH 7.4, using Amicon Ultra 15 concentrators (Millipore). The enzymes concentration was determined using an ε_M of 1.42 x 10^5 $M^{-1}cm^{-1}$ at 280 nm. PLP content was determined by releasing the coenzyme in 0.1 M NaOH using ε_M of 6600 $M^{-1}cm^{-1}$ at 388 nm [28].

2.4 Size-Exclusion liquid chromatography

Size-exclusion liquid chromatography was applied as further purification step. Samples were loaded on a Superdex 200 (10/300) (GE Healthcare) column equilibrated with 100 mM potassium phosphate buffer pH 7.4, on an Akta FPLC system (GE Healthcare). The run was performed using the same buffer at a flow rate of 0.3 ml/min with detection at 280 nm.

2.5 Determination of solubility level of the AADC variants

E. coli has been used as a model for the expression study of the pathogenic AADC variants. Chemical competent bacteria were transformed with the proper mutagenized plasmid as described in the expression and purification section. Cultures were grown even in the absence or in the presence of 50 μM exogenous PLP and 1 mL of each culture was processed following the same procedure described above. After lysis, samples were treated with DNase (10 U) at room temperature for 30 min. The whole cell extract was separated by centrifugation at 13200 rpm, 10 min, 4°C. Total protein content in the crude cellular lysate was quantified and 15 μg of total protein was run on a 12% (w/w) SDS-PAGE gel. The same amount of a sample consisting of the membrane insoluble pellet of wild-type (WT), P210L, L222P, F237S, W267R and E283A variants was analyzed. Proteins from the gel were transferred on a nitrocellulose membrane by a Mini Trans-Blot cell (Bio-Rad). Membrane was blocked with a 5% (w/w) milk solution at 37°C for 1 hour and, after the washing steps, it was incubated with a 1:200 (v/v) diluted anti-AADC monoclonal antibody solution over night at 4°C. Membrane was then washed and then incubated with a 1:4000 (v/v) anti-mouse secondary antibody solution for 1 hour at 25°C. Blotted proteins were detected and quantified with ECL (Millipore), using the ChemiDoc XRS Imaging System (Bio-Rad, Hercules, CA). Quantification of the band was obtained with ImageJ software (Fiji).

2.6 Apoenzyme preparation and coenzyme binding affinity measurements

Apoenzyme was obtained by incubating 5 μM holoenzyme with 10 mM hydroxylamine in 0.5 M potassium phosphate buffer pH 6.8 at 25°C for 3 hours. The solution was then loaded on a Desalting 26/10 column (GE Healthcare) pre-equilibrated with 0.5 M potassium phosphate buffer pH 6.8 and eluted at 1 mL/min. The eluted enzyme was then concentrated on an Amicon Ultra 15 concentrators (Millipore) and washed with 100 mM potassium phosphate buffer pH 7.4.

The equilibrium apparent dissociation constant for PLP, $K_{D(PLP)}$, was determined by measuring the quenching of the intrinsic fluorescence of 0.1 μM AADC apoenzyme incubated in the presence of PLP at concentrations ranging from 0.005 to 20 μM for 3h at 25°C (in the dark) in 100 mM potassium phosphate buffer pH 7.4.

The data were fitted to the following equation:

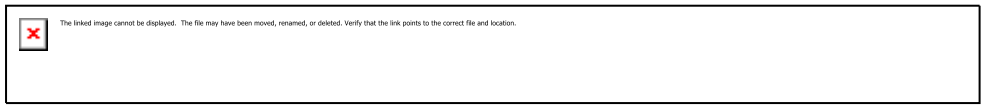

where $[E]_t$ and $[PLP]_t$ represent the total concentrations of the enzyme and PLP, respectively, Y refers to the intrinsic quenching changes at a PLP concentration, and Y_{max} refers to the fluorescence changes when all enzyme molecules are complexed with coenzyme. Curves fitting was performed using Origin® 9.1 Pro (OriginLab).

2.7 Enzyme activity assays

The decarboxylase activity was measured by a stopped spectrophotometric assay [29, 30]. Each variant enzyme (at appropriate concentration) was incubated under saturating PLP concentration (10 μM) and different L-Dopa concentrations in a final volume of 250 μL in 100 mM potassium phosphate buffer pH 7.4 for a time within which a linear product formation is observed. The reaction was then stopped by heating at 100 °C for 2 minutes. TNB (1 ml of a 4.3 mM solution) and toluene (1.5 ml) were added and the extraction of trinitrophenyl-derivative was carried out at 42 °C for 45 minutes with continuous shaking. The concentration of trinitrophenyl-derivative in the toluene layer was quantified using prepared calibration curve of absorbance at 340 nm as a function of trinitrophenyl-derivative concentration [31]. The kinetic parameters were determined by fitting the data obtained with the Michaelis-Menten equation using Origin® 8 Pro (OriginLab).

2.8 Spectroscopic measurements

All spectral measurements were acquired in 100 mM potassium phosphate, pH 7.4, at 25°C. CD measurements were recorded with a Jasco J-710 spectropolarimeter at a scan speed of 50 nm/min with a band width of 2 nm at a protein concentration of 1-5 μM and 10 μM of exogenous PLP for the holoenzymes. Thermal denaturation was performed by monitoring the CD signal at 222 nm of 4 μM enzyme on a 25-90°C linear temperature gradient, with a temperature slope of 1°C/min. Intrinsic fluorescence emission spectra were monitored using a FP-750 Jasco spectrofluorometer at a protein concentration of 1 μM setting at 5 nm excitation and emission bandwidths upon excitation at 280 nm.

2.9 Dynamic Light Scattering (DLS)

Aggregation study was performed on a Zetasizer Nano ZS instrument (Malvern) with a constant 90° scattering angle and a 633 nm wavelength laser. Protein samples were prepared at 4 μM concentration under physiological conditions (58 mM potassium phosphate, pH 7.4 at 37 °C). The

buffer was filtered immediately before the use.

2.10 HPLC analysis of coenzyme modification and dopamine formation

Catalytically inactive AADC variants were incubated at 10 μM protein concentration with 2 mM L-Dopa in 100 mM potassium phosphate buffer, pH 7.4 at 25°C. Concentration-time curves were followed by withdrawing aliquots at time intervals and quenching the reaction by adding trichloroacetic acid to a final concentration of 10% (v/v). Proteins were then precipitated in ice and removed by centrifugation. Supernatants were analyzed by HPLC as described [32] using a Gemini C18 column (150 x 4.6 mm, Phenomenex, CA, USA) and performed on a Jasco PU-2080 Plus HPLC system equipped with a UV-1570 detector set at 295 nm. Samples were eluted in 50 mM potassium phosphate, pH 2.35, at a flow rate of 1 mL/min. Standard curves of peak area as a function of coenzyme or cyclic adducts concentration were prepared with commercially available PLP and coenzyme adducts obtained by synthesis.

2.11 NMR experiments

Before NMR analysis, the HPLC-purified compounds were exchanged in water, lyophilized and re-dissolved in D_2O. All the NMR spectra were recorded at 298 K on a 600 MHz Bruker AVIII HD spectrometer equipped with a TCI cryogenic probe. For the acquisition we used a spectral width of 20 ppm, an acquisition time of 1.36 s, 32000 data points and 128 or 256 scans. NMR data were processed with Topspin 3.2. PLP and PMP peak assignments were confirmed by comparing the chemical shifts of the 1D 1H-NMR spectra with those from reference spectra deposited in the Biological Magnetic Resonance Data Bank (BMRB). The 1H-NMR peak assignments to the Pictet-Spengler adduct were verified by comparing the chemical shifts with previously reported resonances [33] and supported by 2D correlation NMR experiment (TOCSY).

2.12 Limited proteolysis in presence of the substrate analogue DME

Protection studies against tryptic proteolysis were performed as described [32]. WT AADC and variants were incubated with the substrate analogue DME at concentration of 2 mM for 30 seconds, 10 minutes and 30 minutes and then digested with trypsin for 10 minutes at the 1:50 (w/w) ratio. Proteolysis was stopped with the addition of trypsin inhibitor at the 1:10 (w/w) ratio and the reaction samples were then analyzed on a 10% (w/w) SDS-PAGE gel.

2.13 Bioinformatics analyses

Human AADC sequence was aligned with 75 homologues sequences retrieved form Uniref-90 database by the homolog search algorithm PSI-BLAST and aligned using Multiple Sequence Alignment software CLUSTALW on ConSurf server (http://consurf.tau.ac.il). A conservation score (9= highly conserved, 1= highly variable) was attributed to each residue. Structural analysis and *in silico* mutagenesis of the pig DDC (PDB: 1JS6 ; ~90% sequence identity with the human homologous) was carried out using Pymol 2.0 (The PyMOL Molecular Graphics System, Version 2.0 Schrödinger, LLC.). BindProfX was used to predict changes in binding affinity upon mutations in the form of ΔΔG (change in free energy of binding) values. The algorithm combines the FoldX physics-based potential with the conservation scores from pairs of protein-protein interaction surfaces sequence profiles. Interface residues and solvent accessible area (ASA) have been determined starting from the available crystal structure of pig DDC (PDB: 1JS6) by means of the Protein interfaces, surfaces and assemblies' service PISA at the European Bioinformatics Institute (http://www.ebi.ac.uk/pdbe/prot_int/pistart.html)[34].

3. Results

3.1 Solubility and purification yields of the new AADC variants

The 13 new AADC variants were examined for their presence in the soluble fraction. Soluble V60A, H70Y, F77L, G96R, A110E, F251S, L353P and R453C levels are similar with respect to the WT (more than 70%), while P210L, L222P, F237S, W267R and E283A are poorly expressed in the soluble fraction (10-30%) (**Fig 2**). The addition of PLP did not significantly improve expression of either the WT or the variants. A low expression level might be related to a solubility alteration at least in *E. coli* system, suggesting folding defects for low expressed variants.

The insoluble fractions of the poorly expressed variants show that the amount of protein recovered in the pellet is slightly higher as compared to that of the WT (**Fig S1**). However, considering the high soluble/insoluble ratio of WT AADC expressed in *E. coli* system, even subtle differences in insoluble fractions might be indicative of high differences in protein solubility.

Considering the protein yields after purification, some variants exhibit nearly good to good yields (30-85% with respect to the WT), including A110E, L353P, R453C, F251S, F77L and G96R. Others display low (5-10% for V60A and H70Y) and very low (less than 2% for E283A, P210L and W267R) yields. Unfortunately, it was not possible to purify L222P and F237S which were recovered in extremely low amounts (0.3%) preventing us to carry out a complete biochemical characterization.

3.2 Aggregation of apoP210L and apoE283A

Given the great variability in both solubility level and purification yield of the analyzed variants (already reported in sporadic cases for other characterized AADC variants [25, 35-37]), DLS analyses were carried out in order to evaluate the aggregation propensity of the purified enzymes under physiological conditions (58 mM potassium phosphate buffer, pH 7.4 at 37°C). DLS measurements of the holo and apo forms of the majority of AADC variants and of WT **(Fig. 3A)** do not show signs of aggregation suggesting that the enzyme is not prone to aggregate under these experimental conditions. Instead, apoP210L and apoE283A, even if at different extent, tend to aggregate as demonstrated by both the increase in kcps and the disappearance of the dimeric species (**Fig. 3B and 3C**). While dimeric apoE283A disappears in about 300 min, apoP210L aggregation process is much slower. This led us to conclude that some AADC variants in their apo form are prone to undergo an aggregation process.

3.3 Secondary structure and thermal stability of the new AADC variants

The structural integrity of all variants in terms of secondary structure has been evaluated by measuring the far-UV CD spectra of all purified variants in the 190-260 nm region. The signals are superimposable to that of the WT indicating that the substitutions do not alter the secondary structure of the protein (data not shown). In order to determine the intrinsic stability, we measured the T_m's of holo and apo forms of all variants (**Table 2**) by following the loss of the dichroic signal at 222 nm under physiological conditions (58 mM potassium phosphate buffer, pH 7.4).

As for the holo proteins, the value of T_m for F251S, W267R, L353P and R453C is almost identical to that of the WT. Instead, the ΔT_m value ($T_{m(variant)}$-$T_{m(WT)}$) is consistently lower for V60A, A110E and E283A followed by F77L, G96R, H70Y and, to a lesser extent, P210L.

The apo species of V60A, G96R and E283A evidence a marked decrease in T_m with respect of the WT, followed by L353P, P210L, F77L and A110E, while the others exhibit ΔT_m of ± 2°C.

It is interesting to note that the $\Delta T_{m(holo-apo)}$ for the WT is of about 5 °C. This value, indicative of the different thermal stability of the holo and the apo form, is maintained (or even increased) for all variants but V60A, H70Y, F77L, A110E, and R453C.

3.4 Aromatic amino acids dichroic and fluorescence signals and coenzyme dichroic microenvironment features of the new AADC variants

We then measured signals, collected by near UV-CD and intrinsic fluorescence, related to aromatic amino acids environment to monitor possible folding alterations in AADC variants. The near UV-CD at 280 nm provides insight into asymmetric aromatic amino acid residues, mainly tryptophan(s), located in an appropriate position, and is linked to a proper protein tertiary structure arrangement. While the holo forms of G96R, P210L, F251S, and E283A have a 280 nm CD signal very similar to that of the WT, the other variants exhibit decreases in the intensity of the 280 nm band, although at different extent, particularly relevant in V60A, F77L and A110E (**Fig. 4A and 4B**). Since the apo form has a spatial arrangement different from the holo one [27], it is useful to compare the 280 nm CD signals of the apo variants in order to better understand how substitutions exert their effects on the entire protein structure or if the modifications are confined to the PLP binding region. An analysis of the CD near UV bands of the apo forms (**insets of Fig. 4A and 4B**) reveals that they are almost superimposable to that of the WT, unless a subtle decrease of the 280 nm band in G96R, F251S and E283A and a more evident one in V60A and R453C.

Interestingly, the signals in the near UV region of the holo forms of V60A, F77L, and A110E are not so much different from the corresponding ones in the apo species.

The intrinsic fluorescence signal is measured to provide insight into the correct folding features of the enzyme. Following excitation at 280 nm, the fluorescence spectrum of holo WT is characterized

by an emission spectrum with a maximum at 332 nm indicative of the buried environment of the aromatic amino acid residues (**Fig. S2**). Those variants displaying a decrease of the 280 nm CD band present in general an emission band higher than that of the WT, while the 332 nm fluorescence emission is similar to that of the WT for the other variants whose 280 nm CD band is identical or similar to that of the WT. Considering that consistent alterations of tertiary structure were found mainly in the holo forms, the deleterious effects of mutations are reasonably due to an impairment in the correct holo folding rather than to the achievement of the spatial structure of the apo form.

It should be remembered that the apo WT emits at nearly the same wavelength as the holo but with higher intensity values given to different position of aromatic amino acids in this structure or to the energy transfer process from aromatic side chains fluorophores to the pyridine ring of the cofactor. This suggests that some variants remain in a sort of apo structure being somewhat prevented in the apo-to-holo transition or in the acquirement of a correct holo folding, as evidenced above.

Altogether, these spectroscopic results witness slight alterations in global protein folding of the new variants.

As for possible coenzyme microenvironment modifications, we measured the visible CD spectrum of all species. WT AADC presents two bands centered at 335 nm and 420 nm indicative of a tautomeric equilibrium between the enolimine and the ketoenamine forms of the internal aldimine that PLP forms with Lys-303. The spectra of the new variants display small differences with respect to the WT. In details, the spectra of H70Y, G96R, F251S and L353P are similar to that of the WT, while P210L and E283A exhibit a 420 nm band lower than the corresponding one of the WT. On the contrary, V60A, F77L, A110E and R453C show a predominance of the ketoenamine over the enolimine tautomer **(Fig. 4A and 4B**). Since this tautomeric equilibrium is unrelated with catalytic efficiency (see below), these results only reveal subtle PLP microenvironment modifications influencing the tautomeric equilibrium of the internal aldimine.

3.5 Kinetic parameters and apparent PLP equilibrium dissociation constants, $K_{D\ PLP}$, of new AADC variants

The purified variants were functionally characterized by measuring their kinetic parameters. It could be observed (**Table 3**) that the catalytic efficiencies of P210L, F251S and E283A are not so much affected being 52%, 31% and 31%, respectively, compared to that of the WT. These values are due to a small decrease in k_{cat} and nearly equal K_m values for P210L, while in F251S and E283A the decrease of k_{cat} is negligible with respect to that of the WT and K_m is slightly increased.

W267R exhibits a catalytic efficiency value of 15% with respect to WT caused by a decrease in k_{cat} of about 70% and an increase in K_m of about 1.7-fold.

The other variants (V60A, H70Y, F77L, G96R and R453C) are characterized by a marked decrease in catalytic efficiency. This drop is due to a concomitant strong decrease in k_{cat} (mainly for V60A and H70Y) and increase in K_m (mainly for G96R) or both (F77L and R453C). Notably, A110E and L353P are catalytically incompetent under the standard assay conditions.

As for the coenzyme binding affinity, while the $K_{D\ PLP}$ is almost invariant for H70Y and P210L, it increases by 2 up to 5-fold in F77L, G96R, F251S, W267R and L353P and by 6 up to 10-fold in V60A, A110E, E283A and R453C. Thus, the cofactor in many variants is mispositioned and its contacts with the protein moiety are somewhat altered, as also witnessed by the visible CD signals.

3.6 Some AADC variants convert PLP into cyclic Pictet-Spengler adduct in the presence of L-Dopa

Among the variants, A110E and L353P seem to be severely impaired in catalysis since the kinetic parameters could not be measured under the standard assay conditions. Noteworthy, the addition of L-Dopa to both A110E and L353P leads to a decrease of the 420 nm absorbance band and an increase of the 335 nm band that slightly shifts to 329 nm with time. These absorbance bands are associated with the coenzyme bound at the active site. The spectral modifications are indicative of a reaction determining the conversion of the external aldimine between PLP and L-Dopa into an intermediate absorbing at ~ 330 nm, already observed for other AADC variants [35, 38] located in proximity of the active site and attributed to the Pictet-Spengler adduct [33]. The process is faster in A110E and slower in L353P (**Fig. 5A and 5B**). A reaction mixture containing 10 μM A110E or 10 μM L353P with 2 mM L-dopa has been treated and subjected to HPLC analysis, as reported in Materials and Methods section. As shown in **Fig. 5C and 5D**, in both cases the PLP content decreases with an initial rate similar to that of the increase of the Pictet-Spengler cyclic adduct [32, 33]. **Table 4** shows the initial velocities, measured as slopes in the linear part of each curve (PLP decrease and Pictet-Spengler increase) for the two variants in comparison with free PLP under the same experimental conditions. It should be noted that a small amount of dopamine is also produced by both variants (**Table 4**). Given the fact that WT forms dopamine in the presence of saturating L-Dopa (2 mM) with an initial velocity of 7.6 nanomol/sec/nanomol of enzyme (**Table 3**), it follows that the initial velocity of A110E is approximately $7.6 \bullet 10^4$ times and that of L353P of $6.8 \bullet 10^3$ times slower than that of the WT value under the same experimental conditions. It should be noted that, in the case of L353P, a small aliquot of pyridoxamine 5'-phosphate (PMP) is formed, due to the ability of AADC to catalyze multiple side reactions in addition to the main decarboxylation one [33].

While free PLP incubated with L-Dopa forms the cyclic adduct with an initial rate faster than in the two variants (**Table 4**), WT AADC does not form it since the protein moiety prevents unwanted reactions of its highly reactive coenzyme. This suggests that in both A110E and L353P the altered enzyme active site structure renders PLP rather free. The identification of the Pictet-Spengler adduct between L-Dopa and PLP was confirmed by NMR analyses [33] (**Fig. S3)**. In order to check if the active site of the two catalytic variants is somewhat open or not capable of attaining the correct closed and catalytically competent conformation, we added to WT, A110E and L353P the substrate analog DME that binds to PLP but is unable to undergo decarboxylation. At the indicated times (**Fig. 6**), we subjected the enzyme-analog complex to limited proteolysis to monitor the extent of protection. It has been already demonstrated that [33] a protection from proteolysis is indicative of active site correct closure and productive catalysis. While WT does protect from proteolysis, both A110E and L353P do not protect, suggesting that some structural elements of the active site are altered and the closed catalytically competent conformation could not be attained.

3.7 Bioinformatic analyses

In order to verify the conservation level of the newly identified residues of AADC undergoing pathogenic substitution, the AADC amino acid sequence was aligned with those of 75 homologous proteins by the ConSurf web server. About 60% of the modified residues are highly conserved (His-70, Phe-77, Ala-110, Leu-222, Phe-251, Trp-267, Glu-283 and Leu-353). Phe-237 is quite conserved and substituted only by apolar residues or amino acids endowed by a π-system. The others have a low conservation score, although the chemical nature of the residues (polar or apolar) is maintained for Val-60, Gly-96 and Pro-210, while Arg-453 resulted more prone to be substituted by several amino acids in homologous enzymes (**Table S2**).

A bioinformatic analysis examining the arrangement of each residue undergoing substitution was then carried out to understand the *in-silico* impact of each substitution on protein structure and/or binding networks (**Fig. 7A**).

Each monomer of AADC is composed of three domains: the N-terminal domain (residues 1-85) which comprises the structural element loop1 (residues 66-84), the large domain (residues 86-360), which in turn includes loop2 (residues 100-110), the PLP-Lys-303 loop (residues 300-310) and loop3 (residues 323-357, containing the flexible catalytic loop 328-339), and, finally, the C-terminal domain (residues 361-480) [26, 27]. In the holo dimer the two monomers are strictly intertwined leading to a large interlocked interface and, as for the active site, the flexible catalytic loop together with loop1 of each subunit directly interacts with elements of the loops2 and 3 of the neighbouring one [27]. As for the role played by these key loops: loop1 is located in proximity to

the active site and is involved in the apo-to-holo conformational change of AADC [27], loop2 hosts residues near the active site, possibly interacting with the substrate moiety [25, 26], and loop3 is functionally essential for catalysis [26, 27, 31, 39].

Starting from the N-terminal stretch, Val-60 contributes to the monomer-monomer interface and its side chain engages the helix 85-99, that connects loop1 to loop2, of the neighbouring subunit by several hydrophobic contacts (**Fig 7B**). V60A modification reduces the inter-chain hydrophobic contacts within the two N-terminal regions of the AADC dimer. Moreover, the mispositioning of the helix 52-67, due to the substitution of Val-60 with Ala, affects the conformation of loop1. His-70 and Phe-77 belong to loop1. In particular, His-70 side chain interacts with Tyr-20 by an H-bond linkage, while Phe-77 is involved mainly in a base-stacking interaction with the Phe-448 side chain (**Fig 7C**). Together His-70 and Phe-77 represent two anchoring points of loop1 and, of course, of the N-terminal and to the C-terminal domain influencing loop1 correct positioning.

Gly-96 belongs to helix 85-99 at the end of loop1 and just before the beginning of loop2 (**Fig 7B**). Its backbone oxygen interacts with the Asn-308 side chain of the adjacent monomer in proximity of the active site. The G96R substitution could generate a consistent steric hindrance between the two antiparallel helices 85-99 probably perturbing the dimer assembly and the active site.

Ala-110 is the last residue of loop2, belongs to the monomers interface and is placed into an apolar cavity (**Fig 7D**) at the beginning of the large domain. Its substitution with glutamate generates local steric hindrance between the two subunits and seems to exert some effects on the position of residues present at the active site (i. e. Phe-103 and Ile-101, that face PLP, and are part of loop2). This is corroborated by results obtained in the biochemical characterization and the molecular dynamics simulation of the recombinant A110Q protein [25].

Pro-210, Leu-222, Phe-237 and Trp-267 belong to a β-barrel-helices system of the large domain that surrounds the active site. Such complex architecture is highly conserved in the large domain of PLP-dependent enzymes. In details, Pro-210 is placed on a flexible surface stretch (aa 209-218) joining a β-strand to a surface α-helix (**Fig 7E**). The P210L substitution exposes a hydrophobic residue on the protein surface probably inducing local structural rearrangement. Leu-222 belongs to the α-helix 218-232 and lies into a hydrophobic cleft (**Fig 7E**). The exchange to Pro could alter, or even interrupt, the α-helix folding causing a dramatic structural effect. Phe-237 and Trp-267 lie on two adjacent β-sheet elements and are involved in several hydrophobic contacts contributing to the folding features of the β-barrel (**Fig 7F**). It can be expected that the drastic changes of polarity and dimension of the residues introduced by the F237S or W267R substitutions could affect the proper folding of the β-strand/helices packaging.

Phe-251 lies on the loop 243-252 in proximity of the protein surface and takes place to a hydrophobic network involving residues of the large and C-terminal domains (**Fig 7G**). The substitution F251S does not generate significant steric hindrance but it is expected to abolish most of the hydrophobic contacts.

Glu283 is exposed on the protein surface and contacts by a salt bridge the Arg379 side chain (**Fig 7H**). This interaction represents the only connection between the helix 283-294 and the helix 372-395 and, on the basis of the local microenvironment, might prevent the exposure of hydrophobic residues to the solvent. The E283A substitution abolishes such interaction and therefore generates a local conformational change by altering the relative position of surface secondary structure elements.

Leu-353 belongs to loop3 of the large domain, and, in particular, is placed at the dimer interface, near the active site, at a proper distance to interact by hydrophobic contact with two residues: Phe-103, a residue essential for the active site conformation [26] and Arg-347, a key catalytic residue [25, 31] (**Fig 7D**). This network is established in a region critical for catalysis and the substitution of Leu with Pro might determine deep effects on the active site architecture.

Lastly, Arg-453, even if it belongs to the C-terminal domain, provides an additional junction between the C-terminal domain and the loop1, in fact the arginine side chain interacts with the Ser-84 backbone oxygen through an H-bond (**Fig 7C**) and would favour loop1 correct conformation. Moreover, Arg-453 side chain is in proper position to interact with Met-1 backbone oxygen of the neighbouring subunit by a H-bond contributing to the monomer-monomer interaction.

Considering that a significant number of the new mutations are localized at the dimer interface (V60A, G96R, A110E, L353P and R453C), we predicted the values of $\Delta\Delta G$ of the monomer-monomer interaction of WT AADC and of all interface variants using BindProfX (**Table S3**). Results indicate that, even if at different extent, all the interface mutations significantly destabilize the AADC dimer interface.

4. Discussion

In an effort to understand the molecular bases of AADC deficiency, our biochemical approach is aimed to unravel the structure-function relationships of the so-far identified variants in order to elucidate the enzymatic phenotypes. The present study is focused on 13 new pathogenic variants of AADC reported in literature from 2014 to 2019 in homozygosis and hemizygosis. At a first glance, it can be observed that these new amino acid substitutions are spread on the entire protein and not only in the central belt as the previously characterized mutations [25]. Until now, the previously

studied enzymatic phenotypes resulted in impaired apo-to-holo transition and catalysis [25, 31, 35, 40].

Following the investigations previously published [25], the loop1 variants H70Y and F77L resemble, in terms of catalytic efficiency and of structural conformation, the already studied ones affecting loop1 [25]. They are characterized by a drop in k_{cat} and in catalytic efficiency. Less evident are the effects regarding $K_{D(PLP)}$. This behaviour is reasonably due to a stabilizing function of this region [25], whose alteration causes perturbation of both protein conformation and active site architecture. Moreover, the ΔT_m's values with respect to the WT of both holo and apo proteins are notable and the holo-to-apo T_m's difference is diminished with respect to the WT, evidencing that substitutions in loop1 are characterized by a lesser variation in terms of degrees, arguing that these enzymatic species resemble apo rather than holo structures, as also shown by their spectroscopic signals. Interestingly, the clinical phenotypes of patients carrying these mutations are severe [10, 13]. Overall, these new data support the fact that loop1 is crucial for apo-holo transition as suggested by [25].

In addition to this, the remaining newly characterized variants allowed us to widen the spectrum of enzymatic phenotypes related to AADC deficiency. In particular, an interesting cluster of variants is represented by those belonging to the large domain (P210L, L222P, F237S, F251S, W267R and E283A). The bioinformatic analysis reveals that these residues are located either on the surface (P210L, F251S and E283A) or in hydrophobic environments (L222P, F237S and W267R). Except for F251S (see below), all of them are characterized by a low (or null) recovery in the soluble fraction.

Since their apo near UV CD signals are similar to that of the apo WT and their holo near UV CD as well as intrinsic fluorescence spectra are not so much affected, it follows that these purified proteins do not present deep changes in their global structure. This can be correlated to the good catalytic efficiency as well as the quite high PLP affinity, unless for E283A, displayed by these variants. Thus, another mechanism for the pathogenicity for this class of variants should be considered in addition to the already proposed ones [25]. Indeed, the DLS analysis shows that apoE283A and apoP210L have a tendency to aggregate, while neither WT nor any of the other characterized variants has. Even if the time course of disappearance of the dimeric apoE283A and apoP210L is slow under our experimental conditions, it might represent a signal of a trend for these proteins to undergo an aggregation process in their apo form that in part explains the reason why the expression of these variants is so low. Only a small fraction is thus able to reach a competent state binding the coenzyme and performing catalysis, while the great part undergoes aggregation in the apo form. Notably, in the highly crowded cellular microenvironment the aggregation process might

be reinforced and facilitated, even if we have no information regarding relative rates of aggregation with respect to apo-to-holo transition. Interestingly, these two variants present a large effect of ΔT_m of the holo and apo form with respect to holo and apo WT, suggesting that their structure is more labile. Consistently, the very low T_m value of apoE283A may be correlated with the aggregation propensity of this variant. The bioinformatic analyses support the possible protein misfolding effect caused by these variants. The affected soluble expression level of the other large domain variants suggests possible folding defects, whose process should be studied in a more appropriate cell model, as performed previously [40]. The low expression is also in line with what we have observed for R160W variant [37]. The reported clinical phenotypes of patients carrying these mutations are from mild to severe. Patients with F237S substitution have rather mild manifestations compared to others [12], reaching adulthood and for one of them a successful pregnancy has been reported [41]. The other clinical phenotypes are from intermediate to severe [13, 42], suggesting that alterations in the large domain could give rise to a wide spectrum of disease outputs.

Phe-251 is an exception for this cluster of residues in the large domain since its substitution to Ser gives rise to a protein variant which behaves in a similar way to the already characterized S250F variant [40]. The bioinformatic analysis of F251S shows the modest effect exerted that is in line with the results obtained and with the mildness of the clinical phenotype of the patient [14]. This variant is only slightly affected by the substitution in catalytic parameters, in PLP affinity and in the spectroscopic signals.

Considering the remaining new variants (V60A, G96R, A110E, L353P and R453C), their common feature is the belonging to the large interface of AADC. This interface comprises 144 residues of the total 480 amino acids of each monomer and covers the 27.3% of the total solvent-accessible area (ASA) of each subunit. In comparison, the dimer interface of the prototype of Fold-Type I PLP-enzymes, aspartate aminotransferase, covers only 19.8% of the total ASA. The AADC interface goes through the contact surface of the two subunits crossing different regions from the N-terminal to the large domain and to, finally, the C-terminal. Taken together, interface variants could be distinguished in those showing modest effects on catalysis (V60A, G96R and R453C) or large catalytic drops (A110E and L353P). This is expected since they affect different protein regions and may exert long-range effects acting at the strictly tight monomer-monomer interface of AADC. Since the active sites are at the interface, a defect in this wide part of the protein might affect catalysis and/or coenzyme binding.

The interface variants V60A, G96R and R453C are characterized by a low catalytic efficiency due to low k_{cat} for V60A and R453C and high K_m for G96R. This could be also mirrored by the fact that the affinity for the coenzyme is compromised in V60A and R453C, as well as the environment of

aromatic amino acids, and decreased in G96R. Their ΔT_m variations are similar to those recorded for loop1 variants, however the measured $\Delta\Delta G$ values show that the interaction networks between monomers is here affected. The bioinformatic analyses show that Val-60 and Gly-96 maintain the protein interface and are thus involved in dimer assembly, while the effect of Arg-453 on interface affects N-terminal and loop1 proper positioning. Notably, V60A and G96R display the lowest values of T_m for their apo structures, supporting the stabilizing role for this interface region. The effects for R453C are less pronounced and this might in part be related to the observation that patients with R453C substitution have a milder clinical phenotype than the others of this group [43]. A110E and L353P are interface variants with strong catalytic impairments. Both A110E and L353P exhibit a change in the aromatic amino acid environment even if at a different extent. Moreover, the lack of catalytic activity, the irreversible trapping of the coenzyme into a cyclic inactive form and the incapability of these variants to protect from proteolysis in the presence of the substrate analog DME, witness a direct effect of the substituted residues in the active site. This effect is expected since both residues are located in proximity to critical amino acids at the active site such as Ile-101, Phe-103 and Arg-347. The critical role of Arg-347 has already been discussed [31]. Other AADC variants near the active site have been previously described and were able to perform Pictet-Spengler condensation reaction [35] even if at a slower rate. The $\Delta\Delta G$ value for A110E and L353P is positive and suggests that a proper active site closure depends on a productive dimeric assembly. This alteration is also witnessed by changes in T_m values with respect to the WT of both holo and apo A110E (whose $\Delta T_{m(holo\text{-}to\text{-}apo)}$ in terms of degrees is of only 1°C) and apo L353P. It derives that AADC residues affecting catalysis are positioned not only at the active site but also at the dimer interface affecting elements of the active site directly (such as Leu-353) or by long-range interactions (such as Ala-110). It is not strange that patients bearing these mutations are severely affected [13, 44].

Altogether, the combination of bioinformatic analyses with biochemical data has been useful in defining the behaviour of enzymatic variants and deepens the knowledge on enzymatic phenotypes. We have here characterized a new enzymatic phenotype leading to aggregation of AADC variants that open the way on investigations regarding the variants with the hallmark of being low expressed. Furthermore, we have encountered new types of variants located at the protein interface able to play short-range (L353P) and long-range (V60A, G96R, A110E and R453C) effects at the active site, highlighting the importance of the large interface of AADC in protein proper functioning.

The ultimate aim of our approach is to correlate the position of each mutation occurring in a defined protein region to the severity of the enzymatic phenotype in order to contribute in the understanding of the clinical phenotype.

Funding: The contribution of Agilis Biotherapeutics-PTC and of the AADC Research Trust is gratefully acknowledged.

Acknowledgments: We would like to acknowledge Dr. Serena Zanzoni, Centro Piattaforme Tecnologiche, Università di Verona, for the NMR analyses and Silvia Bianconi for the excellent technical support. We would like to thank Prof. Andrea Mozzarelli for critical reading of the manuscript.

5. Legends to Figures

Fig. 1-New and already identified amino acid substitutions in AADC variants. Ribbons representation of the holo AADC (pdb ID 1JS6). The two monomers are white and light orange, respectively, and PLP molecules are represented as green sticks. Mutation sites of previously characterized variants and new variants are presented as orange and yellow sticks, respectively. Image was rendered by PyMol software (Schrödinger).

Fig. 2- Soluble fractions of WT and variants AADC. Western blot analysis is performed with 10 μg of total protein content from soluble lysates of *E. coli* loaded on 12% acrylamide gel. Each bacteria culture has been grown in absence (-) and presence (+) of exogenous PLP. Determination of the expression levels of each variant was estimated using ImageJ software (Fiji) and is reported in the text as percentage with respect to the WT.

Fig. 3-DLS analyses of apo WT, apo P210L and apo E283A as a function of time.
4 μM apo WT (**A**), apo P210L (**B**) and apo E283A (**C**) are incubated in 58 mM potassium phosphate buffer pH 7.4 at 37°C. Grey open symbols indicate the size of the dimer, solid squares indicate the mean count rate.

Fig. 4-Near UV and visible CD spectra of WT AADC and variants in their holo and apo forms.
The spectra are recorded at 5 μM protein concentration, in 100mM potassium-phosphate buffer, pH 7.4. Spectra of the holo forms are recorded in the presence of 10 μM PLP. (**A**) The holo forms of: WT, F251S, E283A, G96R. (**B**) The holo forms of: WT, P210L, L353P, R453C, H70Y, A110E, V60A and F77L. Spectra of the corresponding apo forms are reported in the insets.

Fig. 5-Absorbance spectra of A110E and L353P in the presence of L-Dopa. To a solution of 10 μM A110E (**A**) and L353P (**B**), L-Dopa has been added and spectra are recorded with time in 100 mM potassium phosphate buffer, pH 7.4 at 25°C. Dotted line: variant without L-Dopa. The arrows indicate the increase at 329 nm and the concomitant decrease at 420 nm with time following addition of 2 mM L-Dopa. Insets: increase of the 329 nm and decrease of the 420 nm signals as a function of time. HPLC analyses results of the reaction mixture of 10 μM A110E (**C**) and L353P (**D**) in the presence of 2 mM L-Dopa in 100 mM potassium phosphate buffer, pH 7.4 at 25°C. PLP (●), Pictet-Spengler PLP-L-Dopa (○), dopamine (▲) and PMP (▽).

Fig. 6-Limited tryptic proteolysis of WT (A), A110E (B) and L353P (C) in the presence of DME. WT, A110E and L353P are incubated at a concentration of 10 μM protein with 2 mM DME for various times and then digested with trypsin for 10 minutes at the trypsin/enzyme ratio 1:50 (w:w). t_0 is the control in the absence of trypsin.

Fig. 7-*In silico* inspection of the mutation sites. Ribbons representation of the holo AADC (pdb ID 1JS6). The two monomers are white and light orange, respectively, loop1 (aa 66-84) is magenta and PLP molecules are represented as green sticks. In each panel: (i) the mutation sites are indicated and represented as yellow sticks; (ii) specific interacting residues are in cyan; (iii) clusters of hydrophobic residues are represented as orange sticks. *residues belonging to the neighboring subunit. Image was rendered by PyMol software (Schrödinger).

Table 1. New reported AADC homozygous or hemizygous variants from 2014 to 2019.

new variant	reference	Note
V60A	Hwu et al., 2017 [13]	in hemizygosis, the other allele produces a protein that ends prematurely at 248 amino acids, with no formation of the active site
H70Y	Manegold et al., 2009 [10]; Gucuyener et al., 2014 [45] Montioli et al., 2014 [25]	homozygous, reported incorrectly as H70T
F77L	www.bioku.org/pnd/home.asp	homozygous, on line submission in database in 2012
G96R	Hwu et al., 2017 [16]	in hemizygosis, the other allele produces a protein that ends prematurely at 248 amino acids, with no formation of the active site
A110E	Ide et al., 2010 [44]; Wassenberg et al., 2010 [46]; Montioli et al., 2014 [25]	homozygous, reported incorrectly as A110Q
P210L	Helman et al., 2014 [42]	in hemizygosis, the other allele has a mutation leading to a premature stop codon
L222P	Helman et al., 2014 [42]	Homozygous
F237S	Leuzzi et al., 2015 [12]	in hemizygosis, the other allele has a mutation leading to a premature stop codon
F251S	Chien et al., 2016 [14]	in hemizygosis, the other allele produces a protein that ends prematurely at 248 amino acids, with no formation of the active site
W267R	R. Pons, personal communication	homozygous, R. Pons, personal communication
E283A	Hwu et al., 2017 [13]	in hemizygosis, the other allele produces a protein that ends prematurely at 248 amino acids, with no formation of the active site
L353P	Hwu et al., 2017 [13]	in hemizygosis, the other allele produces a protein that ends prematurely at 248 amino acids, with no formation of the active site
R453C	Graziano et al., 2015 [43]	homozygous, reported incorrectly as R375C

Table 2: Melting Temperatures of WT AADC and variants. Melting temperature values obtained by following the CD signal at 222 nm and varying the temperature linearly from 25 to 90°C with a slope of 1.5 °C/min.

	T_m (°C)	
Enzyme	**holo**	**apo**
WT	69.42 ± 0.02	64.84 ± 0.03
V60A	62.13 ± 0.02	59.30 ± 0.03
H70Y	65.95 ± 0.04	63.28 ± 0.05
F77L	63.58 ± 0.03	61.70 ± 0.03
G96R	65.64 ± 0.05	58.46 ± 0.04
A110E	63.20 ± 0.05	62.04 ± 0.04
P210L	66.10 ± 0.10	60.91 ± 0.05
L222P	n.d	n.d
F237S	n.d	n.d
F251S	70.49 ± 0.04	63.37 ± 0.06
W267R	70.30 ± 0.10	63.60 ± 0.03
E283A	62.89 ± 0.02	58.66 ± 0.07
L353P	68.10 ± 0.07	60.82 ± 0.03
R453C	69.36 ± 0.03	66.70 ± 0.02

Table 3. Steady-state kinetic parameters and apparent equilibrium dissociation constant, Kd, for PLP of the new AADC variants.

Enzyme	k_{cat} (s^{-1})	K_m (mM)	k_{cat}/K_m (s^{-1} mM^{-1})	$K_{D\ PLP}$ (nM)
WT	7.6 ± 0.1	0.11 ± 0.01	69.1 ± 10	43 ± 12
V60A	0.93 ± 0.02	0.16 ± 0.01	5.8 ± 0.4	252 ± 35
H70Y	0.58 ± 0.09	0.26 ± 0.04	2.2 ± 0.5	70 ± 18
F77L	0.35 ± 0.07	0.51 ± 0.05	0.7 ± 0.1	222 ± 38
G96R	5.7 ± 0.4	3.5 ± 0.4	1.6 ± 0.2	132 ± 14
A110E	n.d.	n.d.	n.d.	321 ± 26
P210L	4.4 ± 0.2	0.12 ± 0.02	37 ± 6	47 ± 7
L222P	n.p.	n.p.	n.p.	n.p.
F237S	n.p.	n.p.	n.p.	n.p.
F251S	5.7 ± 0.2	0.26 ± 0.02	22.0 ± 0.2	88 ± 16
W267R	2.11 ± 0.04	0.19 ± 0.01	11.1 ± 0.6	120 ± 10
E283A	6.4 ± 0.2	0.29 ± 0.05	22.0 ± 0.2	330 ± 30
L353P	n.d.	n.d.	n.d.	199 ± 34
R453C	0.67 ± 0.07	0.40 ± 0.06	1.7 ± 0.3	468 ± 36

n.d., not detectable under standard assay conditions; n.p., not purified

Table 4. Initial velocities of dopamine formation, PLP decrease, Pictet-Spengler and PMP increase following reaction of 10 μM A110E or L353P or 20 μM PLP with 2 mM L-Dopa

initial velocity (v_0) (nmol/min/nmol)	**A110E**	**L353P**	**free PLP**
v_0 dopamine	0.006 ± 0.001	0.067 ± 0.001	--
v_0 PLP decrease	0.040 ± 0.004	0.006 ± 0.002	0.12 ± 0.01
v_0 Pictet-Spengler	0.042 ± 0.006	0.005 ± 0.003	0.10 ± 0.04
v_0 PMP	--	0.002 ± 0.00005	--

6. References

[1] K. Hyland, P.T. Clayton, J Inherit Metab Dis 13 (1990) 301-304
[2] K. Hyland, R.A. Surtees, C. Rodeck, P.T. Clayton, Neurology 42 (1992) 1980-1988
[3] W. Lovenberg, H. Weissbach, S. Udenfriend, J. Biol. Chem. 237 (1962) 5
[4] M. Bertoldi, Arch Biochem Biophys 546 (2014) 1-7 S0003-9861(13)00394-9 [pii]
10.1016/j.abb.2013.12.020
[5] K.J. Swoboda, K. Hyland, D.S. Goldstein, K.C. Kuban, L.A. Arnold, C.S. Holmes, H.L. Levy, Neurology 53 (1999) 1205-1211
[6] R. Pons, B. Ford, C.A. Chiriboga, P.T. Clayton, V. Hinton, K. Hyland, R. Sharma, D.C. De Vivo, Neurology 62 (2004) 1058-1065
[7] G.F. Allen, J.M. Land, S.J. Heales, Mol Genet Metab 97 (2009) 6-14 S1096-7192(09)00010-9 [pii]
10.1016/j.ymgme.2009.01.010
[8] L. Brun, L.H. Ngu, W.T. Keng, G.S. Ch'ng, Y.S. Choy, W.L. Hwu, W.T. Lee, M.A. Willemsen, M.M. Verbeek, T. Wassenberg, L. Regal, S. Orcesi, D. Tonduti, P. Accorsi, H. Testard, J.E. Abdenur, S. Tay, G.F. Allen, S. Heales, I. Kern, M. Kato, A. Burlina, C. Manegold, G.F. Hoffmann, N. Blau, Neurology 75 (2010) 64-71 WNL.0b013e3181e620ae [pii]
10.1212/WNL.0b013e3181e620ae
[9] T. Wassenberg, M. Molero-Luis, K. Jeltsch, G.F. Hoffmann, B. Assmann, N. Blau, A. Garcia-Cazorla, R. Artuch, R. Pons, T.S. Pearson, V. Leuzzi, M. Mastrangelo, P.L. Pearl, W.T. Lee, M.A. Kurian, S. Heales, L. Flint, M. Verbeek, M. Willemsen, T. Opladen, Orphanet J Rare Dis 12 (2017) 12 10.1186/s13023-016-0522-z
10.1186/s13023-016-0522-z [pii]
[10] C. Manegold, G.F. Hoffmann, I. Degen, H. Ikonomidou, A. Knust, M.W. Laass, M. Pritsch, E. Wilichowski, F. Horster, J Inherit Metab Dis 32 (2009) 371-380 10.1007/s10545-009-1076-1
[11] S. Portaro, A. Gugliandolo, D. Scionti, S. Cammaroto, R. Morabito, S. Leonardi, F. Fraggetta, P. Bramanti, E. Mazzon, Medicine (Baltimore) 97 (2018) e10953 10.1097/MD.0000000000010953
00005792-201806010-00069 [pii]
[12] V. Leuzzi, M. Mastrangelo, A. Polizzi, C. Artiola, A.B. van Kuilenburg, C. Carducci, M. Ruggieri, R. Barone, B. Tavazzi, N.G. Abeling, L. Zoetekouw, V. Sofia, M. Zappia, JIMD Rep 15 (2015) 39-45 10.1007/8904_2014_295
[13] W.L. Hwu, Y.H. Chien, N.C. Lee, M.H. Li, JIMD Rep (2017) 10.1007/8904_2017_54
[14] Y.H. Chien, P.W. Chen, N.C. Lee, W.S. Hsieh, P.C. Chiu, W.L. Hwu, F.J. Tsai, S.P. Lin, S.Y. Chu, Y.J. Jong, M.C. Chao, Mol Genet Metab 118 (2016) 259-263 S1096-7192(16)30086-5 [pii]
10.1016/j.ymgme.2016.05.011
[15] N. Himmelreich, R. Montioli, M. Bertoldi, C. Carducci, V. Leuzzi, C. Gemperle, T. Berner, K. Hyland, B. Thony, G.F. Hoffmann, C.B. Voltattorni, N. Blau, Mol Genet Metab (2019) S1096-7192(18)30786-8 [pii]
10.1016/j.ymgme.2019.03.009
[16] W.L. Hwu, S. Muramatsu, S.H. Tseng, K.Y. Tzen, N.C. Lee, Y.H. Chien, R.O. Snyder, B.J. Byrne, C.H. Tai, R.M. Wu, Sci Transl Med 4 (2012) 134ra161 4/134/134ra61 [pii]
10.1126/scitranslmed.3003640
[17] Y.H. Chien, N.C. Lee, S.H. Tseng, C.H. Tai, S.I. Muramatsu, B.J. Byrne, W.L. Hwu, Lancet Child Adolesc Health 1 (2017) 265-273 S2352-4642(17)30125-6 [pii]
10.1016/S2352-4642(17)30125-6

[18] N.C. Lee, Y.H. Chien, W.L. Hwu, Am J Med Genet C Semin Med Genet (2019) 10.1002/ajmg.c.31670
[19] C.H. Tseng, Y.H. Chien, N.C. Lee, Y.C. Hsu, S.F. Peng, W.I. Tseng, W.L. Hwu, Ann Neurol 85 (2019) 644-652 10.1002/ana.25467
[20] K. Kojima, T. Nakajima, N. Taga, A. Miyauchi, M. Kato, A. Matsumoto, T. Ikeda, K. Nakamura, T. Kubota, H. Mizukami, S. Ono, Y. Onuki, T. Sato, H. Osaka, S.I. Muramatsu, T. Yamagata, Brain 142 (2019) 322-333 5296575 [pii]
10.1093/brain/awy331
[21] C. Caine, M. Shohat, J.K. Kim, K. Nakanishi, S. Homma, E.V. Mosharov, U.R. Monani, Hum Mol Genet 26 (2017) 4406-4415 4090955 [pii]
10.1093/hmg/ddx326
[22] N.C. Lee, Y.D. Shieh, Y.H. Chien, K.Y. Tzen, I.S. Yu, P.W. Chen, M.H. Hu, M.K. Hu, S. Muramatsu, H. Ichinose, W.L. Hwu, Neurobiol Dis 52 (2013) 177-190 S0969-9961(12)00388-9 [pii]
10.1016/j.nbd.2012.12.005
[23] M.Z. Zhang, B. Yao, S. Wang, X. Fan, G. Wu, H. Yang, H. Yin, S. Yang, R.C. Harris, J Clin Invest 121 (2011) 2845-2854 57324 [pii]
10.1172/JCI57324
[24] S.Y. Ho, Y.H. Chien, L.K. Tsai, S.I. Muramatsu, W.L. Hwu, H.H. Liou, N.C. Lee, Front Cell Neurosci 13 (2019) 9 10.3389/fncel.2019.00009
[25] R. Montioli, M. Dindo, A. Giorgetti, S. Piccoli, B. Cellini, C.B. Voltattorni, Hum Mol Genet 23 (2014) 5429-5440 ddu266 [pii]
10.1093/hmg/ddu266
[26] P. Burkhard, P. Dominici, C. Borri-Voltattorni, J.N. Jansonius, V.N. Malashkevich, Nat Struct Biol 8 (2001) 963-967 10.1038/nsb1101-963
nsb1101-963 [pii]
[27] G. Giardina, R. Montioli, S. Gianni, B. Cellini, A. Paiardini, C.B. Voltattorni, F. Cutruzzola, Proc Natl Acad Sci U S A 108 (2011) 20514-20519 1111456108 [pii]
10.1073/pnas.1111456108
[28] E.A. Peterson, H.A. Sober, Journal of American Chemical Society 76 (1954) 7
[29] A.F. Sherald, J.C. Sparrow, T.R. Wright, Anal Biochem 56 (1973) 300-305 0003-2697(73)90194-2 [pii]
[30] A. Charteris, R. John, Anal Biochem 66 (1975) 365-371 0003-2697(75)90604-1 [pii]
[31] R. Montioli, A. Paiardini, M.A. Kurian, M. Dindo, G. Rossignoli, S.J.R. Heales, S. Pope, C.B. Voltattorni, M. Bertoldi, Biochim Biophys Acta 1864 (2016) 676-682 S1570-9639(16)30053-X [pii]
10.1016/j.bbapap.2016.03.011
[32] M. Bertoldi, C. Borri Voltattorni, Biochem J 352 Pt 2 (2000) 533-538
[33] M. Bertoldi, P. Frigeri, M. Paci, C.B. Voltattorni, J Biol Chem 274 (1999) 5514-5521
[34] E. Krissinel, K. Henrick, J Mol Biol 372 (2007) 774-797 S0022-2836(07)00642-0 [pii]
10.1016/j.jmb.2007.05.022
[35] R. Montioli, B. Cellini, C. Borri Voltattorni, J Inherit Metab Dis 34 (2011) 1213-1224 10.1007/s10545-011-9340-6
[36] R. Montioli, G. Janson, A. Paiardini, M. Bertoldi, C. Borri Voltattorni, IUBMB Life 70 (2018) 215-223 10.1002/iub.1718
[37] R. Montioli, R. Battini, A. Paiardini, M. Tolve, M. Bertoldi, C. Carducci, V. Leuzzi, C. Borri Voltattorni, Mol Genet Metab 127 (2019) 132-137 S1096-7192(19)30245-8 [pii]
10.1016/j.ymgme.2019.05.004
[38] R. Montioli, R. Battini, A. Paiardini, M. Tolve, M. Bertoldi, C. Carducci, V. Leuzzi, C. Borri Voltattorni, Mol Genet Metab (2019) S1096-7192(19)30245-8 [pii]
10.1016/j.ymgme.2019.05.004

[39] M. Bertoldi, M. Gonsalvi, R. Contestabile, C.B. Voltattorni, J Biol Chem 277 (2002) 36357-36362 10.1074/jbc.M204867200
M204867200 [pii]
[40] R. Montioli, E. Oppici, B. Cellini, A. Roncador, M. Dindo, C.B. Voltattorni, Hum Mol Genet 22 (2013) 1615-1624 ddt011 [pii]
10.1093/hmg/ddt011
[41] M. Mastrangelo, F. Manti, L. Patane, S. Ferrari, C. Carducci, G. Mangili, V. Leuzzi, Mov Disord Clin Pract 5 (2018) 446-447 10.1002/mdc3.12622
MDC312622 [pii]
[42] G. Helman, M.B. Pappa, P.L. Pearl, JIMD Rep 17 (2014) 23-27 10.1007/8904_2014_327
[43] C. Graziano, A. Wischmeijer, T. Pippucci, C. Fusco, C. Diquigiovanni, M. Noukas, M. Sauk, A. Kurg, F. Rivieri, N. Blau, G.F. Hoffmann, A. Chaubey, C.E. Schwartz, G. Romeo, E. Bonora, L. Garavelli, M. Seri, Gene 559 (2015) 144-148 S0378-1119(15)00042-6 [pii]
10.1016/j.gene.2015.01.026
[44] S. Ide, M. Sasaki, M. Kato, T. Shiihara, S. Kinoshita, J.Y. Takahashi, Y. Goto, Brain Dev 32 (2010) 506-510 S0387-7604(09)00165-X [pii]
10.1016/j.braindev.2009.05.004
[45] K. Gucuyener, C.S. Kasapkara, L. Tumer, M.M. Verbeek, Ann Indian Acad Neurol 17 (2014) 234-236 10.4103/0972-2327.132652
AIAN-17-234 [pii]
[46] T. Wassenberg, M.A. Willemsen, P.B. Geurtz, M. Lammens, K. Verrijp, M. Wilmer, W.T. Lee, R.A. Wevers, M.M. Verbeek, Mol Genet Metab 101 (2010) 349-356 S1096-7192(10)00299-4 [pii]
10.1016/j.ymgme.2010.08.003